Catal Lett (2013) 143:206–218
DOI 10.1007/s10562-012-0923-0

Pd Nanoparticles on Layered Double Hydroxide as Efficient Catalysts for Solvent-Free Oxidation of Benzyl Alcohol Using Molecular Oxygen: Effect of Support Basic Properties

Tao Chen · Fazhi Zhang · Yue Zhu

Received: 23 June 2012 / Accepted: 4 October 2012 / Published online: 27 October 2012

Abstract Pd nanoparticles supported on basic layered double hydroxide (LDH) as highly efficient and reusable catalysts are prepared and characterized. The layered structure of LDH support could be reconstructed to different extent by controlling the activation conditions, which presented changing quantity of Brønsted-base sites. Besides, with the changing calcination temperature the LDH substrate imposed a restricted nano-size effect on the supported Pd particles under identical reduction condition, which demonstrated a convenient approach for controlling the size of supported Pd particles. The resulting Pd/LDH samples were tested as heterogeneous catalysts for solvent-free oxidation of benzyl alcohol using molecular oxygen. The sample with a larger amount of Brønsted-base sites is more active in the oxidation of benzyl alcohol, and after five catalytic runs it still gives benzaldehyde in excellent yields. The promotional effect of Brønsted-base sites of the LDH support on the catalytic activity for benzyl alcohol oxidation over Pd/LDH is studied.

Keywords Heterogeneous catalysis · Nanoparticles · Bifunctionality · Regeneration · Oxidation

Electronic supplementary material The online version of this article (doi:10.1007/s10562-012-0923-0) contains supplementary material, which is available to authorized users.

T. Chen · F. Zhang (✉) · Y. Zhu
State Key Laboratory of Chemical Resource Engineering, Beijing University of Chemical Technology, Beijing 100029, China
e-mail: zhangfz@mail.buct.edu.cn

1 Introduction

Supported metal catalysts are of great importance for the environmentally benign synthesis of bulk and fine chemicals due to easy recyclability and separability. More and more attention of the scientific community has been paid to the effect of support nature on the catalytic performance [1, 2], especially the surface acidic/basic properties, which have been manifested in a variety of reactions including as hydrogenation of nitriles [3–5], hydrogenation of toluene [6, 7], hydrogenation of phenol [8], hydrogenolysis of neopentane [9], and dehydrocyclization of *n*-hexane [10]. Lashdaf et al. [11] also found that the hydrogenation of cinnamaldehyde was significantly influenced by the Brønsted acidity of Pt supported beta zeolite and the activity for the acetal formation increased with the total number of acid sites on the zeolite. Very recently, Hu et al. [12] also reported the crucial role of surface acidity of supported Ni catalysts in the hydrogenation of aromatic rings. More interesting, some catalyzed reactions require the cooperation of additional acid or base with heterogeneous catalysts to fulfill the catalytic cycle efficiently. Liu et al. [13] reported the excellent synergy of supported Pd catalysts with extraneous solid Lewis acid for the hydrogenation of phenol, which exhibited highly activity and selectivity. Zhu et al. [14] researched the promotion of various bases on Au/activated-carbon catalysts for oxidation of benzyl alcohol, which showed the basicity of additional alkali influenced the activity and selectivity significantly. The above research proved that the surface acidic or basic properties of supports play an important role in affecting the catalytic performance of the supported metal particles. Developing new type metal catalysts with controllable surface acidic or basic properties of supports is thus highly valued.

Layered double hydroxide (LDH), whose structure can be described by the general formula $[M^{2+}_{1-x}M^{3+}_{x}(OH)_2]^{x+}[A^{n-}]_{x/n}\cdot yH_2O$, comprises positively charged brucite-like sheets and exchangeable guest anions located in the hydrated interlayer regions for charge balance [15, 16]. Accordingly, the flexibility and diversity in composition give LDH access to a wide-ranging of significant applications including as magnetic materials precursors [17], polymers additives [18], and in electrochemistry [19], biology and medicine chemistry [20], photochemistry [21], and environmental remediation [22, 23]. Particularly, as a consequence of the tailored structure-design and controlled accessibility to catalytic sites [24, 25], LDH provide potential opportunities for designing and innovating novel catalysts and precursors or supports of catalysts. For instance, with high density of Brønsted-base sites proceeding from the brucite-like structure [25], which can be modified by changing the cations in the layers, the M^{2+}/M^{3+} ratio, the nature of compensating anions, and even the activation conditions, LDH as heterogeneous solid base catalysts are currently receiving considerable attention [26, 27]. It is well known that LDH plays a significant role as a solid base catalyst in Knoevenagel condensation, aldol condensation, Claisen–Schmidt condensation, Henry, Wittig, and Michael addition reactions. Herein, we report the research on the remarkable promotional effect of the Brønsted-base sites of the LDH support on the catalytic activity for solvent-free oxidation of benzyl alcohol using molecular oxygen over supported Pd/LDH.

Considering the increasing environmental problems, it is highly desirable to use molecular oxygen or hydrogen peroxide to take the place of traditional corrosive, toxic and expensive oxidants such as manganese and chromium (VI) complexes for the oxidation of alcohols. Most recently, the Pd-based catalysts can be very effective for the oxidation of alcohols to aldehydes, using O_2 under relatively mild conditions. Kaneda and co-workers [28] found that Pd nanoclusters supported hydroxyapatite (Pd/HAP) exhibited highly activity in the oxidation of benzyl alcohol. Enache et al. [2] also reported different substrate-supported Au–Pd catalysts for the oxidation of benzyl alcohol at 100 °C with O_2 in the absence of solvent, and found that different supports give birth to distinct activity and selectivity. Pd pyridine complex $Pd(OAc)_2(py)_2$ immobilized on the external surface of LDH was reported by Uemura and co-workers [29, 30], which was found to be active in the oxidation of benzyl alcohol (TOF up to 10 h^{-1}) in toluene and gave good yield of benzaldehyde. Recently, a Pd^{II} hydroxyl complex intercalated LDH was found to be active for the oxidation of benzyl alcohol (TOF = 50 h^{-1}) [31]. For the aerobic oxidation of alcohols, an exogeneous base is often added into the catalytic system as an efficient promoter, such as pyridine, K_2CO_3 or NaOAc, especially when the support material is not basic, or without any supports [1, 29, 30, 32–37]. The base could facilitate the cleavage of the O–H bond of alcohols to form alkoxide intermediates [37]. LDH owns the particular ability in immobilizing metal nanoparticles or complex and activating the O–H bond of alcohols by basic sites [38], which should make LDH a very popular support in heterogeneous catalysis for benzyl alcohol oxidation. By taking advantage of the attractive feature of Brønsted-base sites proceeding from the LDH support, we herein found that Pd nanoparticles supported on LDH can be an effective heterogeneous catalyst for the solvent-free oxidation of benzyl alcohol using molecular oxygen. The effects of calcination temperature on the size of supported Pd particles and the catalytic performance promoted by the Brønsted-base sites of the LDH support for the benzyl alcohol oxidation are investigated. High selectivity for the benzaldehyde, possibility of easy recycle, and free of basic additives or co-catalysts enable the Pd/LDH catalyst highly desirable to address the industrial needs and environmental concerns.

2 Experimental

2.1 Materials

Chemical reagents such as $Mg(NO_3)_2\cdot 6H_2O$, $Al(NO_3)_3\cdot 9H_2O$, urea, ethanol, and acetone are of analytical purity and used without further purification. Sodium tetrachloropalladate (II) hydrate ($Na_2PdCl_4\cdot 3H_2O$), SiO_2, Al_2O_3, hydrazine hydrate, benzyl alcohol, and *n*-decane are purchased from J&K Chemical Ltd.

2.2 Catalyst Preparation

2.2.1 Preparation of LDH Support

$MgAl–OH^-$–LDH with larger crystallite sizes in the range of microns was prepared following a reported procedure [39]. A solution of $Mg(NO_3)_2\cdot 6H_2O$ and $Al(NO_3)_3\cdot 9H_2O$ dissolved in 75 mL deionized water with Mg^{2+}/Al^{3+} molar ratio of 2.0 and a total concentration of metal cations of 0.3 M, was placed in a polytetrafluoroethylene vessel. Urea ($[urea]/[NO_3^-] = 4.0$) was dissolved in the above solution. The container was sealed and placed in an oven and maintained at 90 °C for 3 days. The resulting solid was heated in a N_2 flow at 500 °C for 8 h and then dispersed in decarbonated water for 5 h, subsequently dried under vacuum, resulting in the OH^- anions intercalated LDH support material.

2.2.2 Preparation of Pd/LDH Catalysts

Supported Pd nanoparticles on LDH catalyst samples (Pd/LDH) were prepared by the well-established impregnation method. In a typical procedure, a known amount of Na_2PdCl_4 with appropriate concentration, which was adjusted to yield catalysts containing 1.06 wt% Pd, was prepared advanced and stored at room temperature. Then, LDH powder was dispersed in the Na_2PdCl_4 solution and under continuous stirring for 12 h at 80 °C. After filtered and extensive washing with deionized water, the samples were vacuum dried at 50 °C overnight, then calcinated at 100, 200, 300, 400, and 500 °C for 5 h in air, respectively. Following, the resulting samples were reduced with hydrazine hydrate (1 g, 20 mmol) in ethanol aqueous solution (1:1, 10 mL) under a nitrogen atmosphere for 5 h at room temperature. The final washing with ethanol gives sample the air-stable black powder. The obtaining Pd/LDH catalyst samples are denoted as C1, C2, C3, C4, and C5 with calcination temperature 100, 200, 300, 400, and 500 °C, respectively. For comparison purpose, inorganic SiO_2 and Al_2O_3 supports were also dispersed in the Na_2PdCl_4 solution and stirred for 12 h at 80 °C. After filtration, washing and drying, the resulting solid were treated similarly with hydrazine hydrate to produce the supported Pd/SiO_2 and Pd/Al_2O_3 catalysts.

2.3 Characterization

Powder X-ray diffraction (XRD) patterns were collected on a Shimadzu XRD-6000 instrument with Cu Kα radiation ($\lambda = 0.154$ nm) in the 2θ range from 3° to 70°. Elemental analyses of Pd were performed by inductively coupled plasma emission spectrometry (ICP-ES) using a Shimadzu ICP-7500 instrument. Scanning electron microscopy (SEM) was recorded on a Zeiss Supra 55 instrument. The powder samples were first dispersed carefully in ethanol using an ultrasonic bath, and then deposited on silicon substrate. High resolution transmission electron microscopy (HRTEM) and TEM images were taken with a JEM-2100 instrument operating at an accelerating voltage of 200 kV. The temperature-programmed reduction (TPR) of H_2 was performed for the samples before reduction using a Micromeritics ChemiSorb 2720 instrument. Typically, the sample (0.1 g) was first pretreated in a quartz reactor by passing an Ar stream with a rate of 40 mL/min at 200 °C for 120 min in order to remove any physisorbed molecules. After the sample was cooled to 20 °C, a H_2/Ar (10 % H_2) mixture was introduced into the reactor and the temperature was raised at a rate of 5 °C/min. The consumption of H_2 was monitored by a thermal conductivity detector (TCD). The temperature-programmed desorption (TPD) of CO_2 and NH_3 were conducted on a TJXQ/TP-5080 equipped with a TCD and the signals were detected after removing the produced water vapour. About 100 mg of samples were loaded in a quartz reactor and heated in He for 180 min at 200 °C, followed by treating with the 3 % probe molecules in He flow (20 mL/min) for 60 min at 80 °C. Weakly adsorbed probe molecules were removed by flowing He for 60 min at 80 °C, and then desorption process was carried out from 80 to 800 °C at 5 °C/min in He flow. The low temperature N_2 adsorption–desorption experiments were carried out using a Quantachrome Autosorb-1C-VP instrument. The Barrett–Joyner–Halenda (BJH) method was used to calculate the pore volume and the pore size distribution. The specific surface area was calculated according to the Brunauer–Emmett–Teller (BET) method based on the adsorption isotherm. X-ray photoelectron spectra (XPS) of the catalysts were recorded with a Thermo Fisher ESCALAB 250 spectrometer equipped with Mg Kα radiation. The binding energies of Pd 3d were corrected for surface charging by referencing them to the energy of C 1s peak of contaminant carbon at 285.0 eV. The catalytic reaction was monitored by a Shimadzu gas chromatography (Rtx-1 capillary column, 30 m–0.25 mm) with flame ionization detector using nitrogen as carrier gas. Both the injector and detector temperature were 250 °C. The resulting products were identified by GC–MS using a HP5790 series mass selective detector.

2.4 Catalytic Reaction Procedure

The solvent-free oxidation of benzyl alcohol over the obtaining Pd/LDH samples was carried out under oxygen by contacting 0.1 g of the samples with 5.0 mL of benzyl alcohol (48.5 mmol) in a magnetically stirred glass reactor equipped with a condenser at the temperature of 100 °C and 600 rpm for an appropriate time. The samples were withdrawn at regular interval and analyzed by GC. The yield and selectivity were calculated on the basis of benzyl alcohol using *n*-decane as an internal standard substance. After the reaction, the catalyst was separated by centrifugation and washed thoroughly with acetone, ethanol, and water. The recovered catalyst was dried under vacuum overnight, and then successively reused for subsequent oxidation of benzyl alcohol for testing the reusability of the catalyst.

3 Results and Discussion

3.1 Structure and Morphology Properties of Pd/LDH Samples

$MgAl–OH^-$–LDH support sample was prepared beforehand with larger crystallite sizes in the range of microns

[39–41]. Figure 1a shows the XRD pattern of LDH support, displaying a series of characteristic reflections (001) of LDH structure with great intensity and narrow linewidth. The non-basal reflections (h, $k \neq 0$) at high angle also indicated the high crystallinity of the LDH precursor, in which the two reflections of (110) and (113) are clearly distinguished between 60° and 63° 2θ. Besides, the basal spacing value ($d_{003} = 0.78$) is closely comparable to that reported in the literature for OH^- anions intercalated MgAl–LDH [39]. The crystallite size in c direction (the stacking direction, perpendicular to the basal layers) for the prepared LDH is estimated to be 23.1 nm from the XRD by Scherrer equation. The series of Pd/LDH catalyst samples were then prepared by the well-established impregnation method. As expected, the characteristic peaks of LDH observed in the XRD of the resulting catalyst samples (Fig. 1b–f) revealed that the magnesium and aluminium coordination modes were restored to the original octahedral hydrotalcite structure. According to the literatures [25, 27], the reconstruction of the lamellar structure of the MgAl–LDH material by rehydration in aqueous solution of calcinated LDH is often described as a "memory effect". As can be seen from Fig. 1, the LDH structure can be regenerated in ethanol aqueous solution for the series of catalyst samples. Peak intensity and sharpness of (003) reflection, which are directly proportional to the crystallinity of samples, were obviously decreasing on the increasing

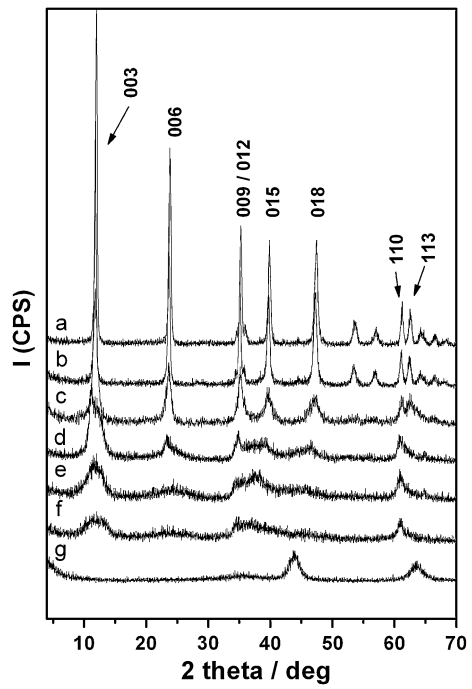

Fig. 1 XRD patterns of the LDH support (**a**) and the resulting Pd/LDH catalysts with different calcination temperature (**b**) C1, (**c**) C2, (**d**) C3, (**e**) C4, and (**f**) C5. The LDH support calcinated at 500 °C without rehydration (**g**)

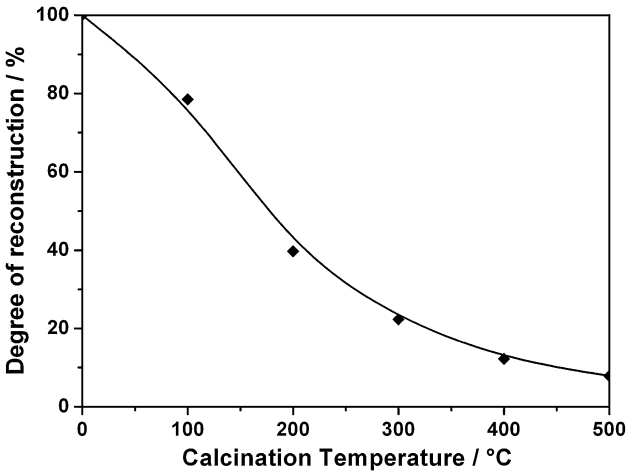

Fig. 2 Degree of reconstruction of the resulting Pd/LDH catalysts with different calcination temperature

calcination temperature. The degree of reconstruction was calculated by comparing the peak intensity of (003) reflection of each catalyst sample with the peak intensity of the LDH support. The original LDH support without calcination was assumed to have highest crystallinity. Degree of reconstruction was observed to decrease linearly (Fig. 2). Also, we note that no characteristic diffraction peaks of Pd can be observed for the Pd/LDH catalyst samples as a low Pd loading of about 1.06 wt%.

Typical SEM images (Fig. 3) were recorded to investigate the morphology of the prepared support and the corresponding catalyst samples. As expected, the micrograph of LDH support (Fig. 3a) shows well-developed hexagonal plates with average crystal sizes ranging among 1–2 μm. Figure 3b–f show the SEM images of the supported Pd/LDH catalysts with different degree of reconstruction. Although the resulting samples underwent calcination with different temperatures from 100 to 500 °C, the morphology of the samples were mostly recovered by following reconstruction in ethanol aqueous solution. The well-developed hexagonal plates of LDH crystallites can be clearly observed, although with some degree of agglomeration of particles.

3.2 Textural and Basic Properties of Pd/LDH Samples

The textural and pore size distribution properties of the series of Pd/LDH samples were analyzed by nitrogen sorption measurement. All the five Pd/LDH samples (Fig. S1a) exhibit a typical IV isotherm with a H1- and H3-type hysteresis loop, implying the presence of mesopores. This result is further confirmed by the corresponding rather uniform distribution of pore size in Fig. S1b, which is generally considered to indicate that the stacking of LDH microcrystallites result in both parallel and tubular slit-shaped capillary

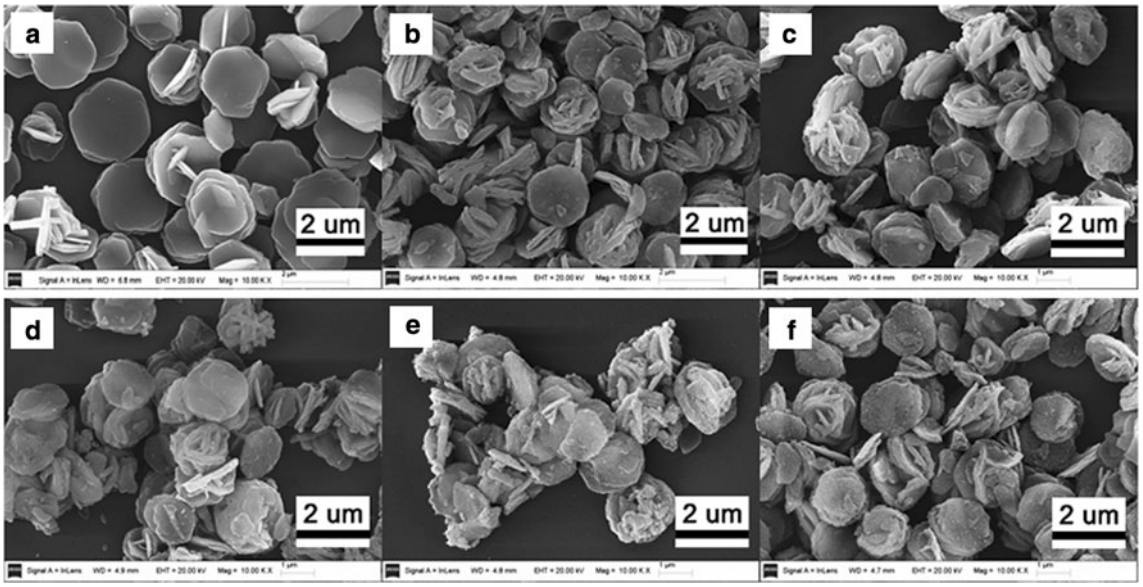

Fig. 3 SEM images of the LDH support (**a**) and the resulting Pd/LDH catalysts (**b**) C1, (**c**) C2, (**d**) C3, (**e**) C4, and (**f**) C5

pores [42]. The corresponding pore size distribution and the specific textural properties of the samples, which undergo different calcination temperature, are listed in Table 1. The pore diameter distribution of C1 sample covers a narrow range, with the most probable pore size at 3.0 nm, which may be a result that fewer particles are aggregated during the calcination due to the relatively low temperature. With the increase of the calcination temperature to 400 °C, Pd/LDH samples show a gradually increasing trend for the specific surface area, most probable pore size, and total pore volume. This may be resulted from the formation of a large number of the shrinked LDH crystallites during the calcination process and the aggregation of the pores in the microcrystallites [15]. However, for the case of C5 sample, the specific surface area and total pore volume are slightly lower than those of C4 sample, which may be caused by the incomplete regeneration of the LDH structure. Based on the above results, we can see that although the series of Pd/LDH samples provide the consistent isotherms, the aforementioned results present distinct difference in the architecture by different calcination temperature and the following reconstruction process, which are attributed to the structure regeneration degree of LDH microcrystallites. This may be crucial for the nature and accessability of the Brønsted-base sites on the LDH surface. The Brønsted (OH^-) basic sites formed by reconstruction method have been reported to be active for aldol condensation reactions, while carbonate intercalated LDH displays no catalytic activity [25, 43, 44]. Under inert atmosphere, the original layered structure of calcined LDH could be regenerated by rehydration in aqueous solution. As a consequence of reconstruction, an efficient solid base catalyst is available owing to the hydroxyl groups as the charge balancing species

Table 1 Physicochemical properties of the Pd/LDH catalysts with different calcination temperature

Sample	S_{BET} (m^2 g^{-1})[a]	V_{total} (cm^3 g^{-1})[b]	D_{BJH} (nm)[c]
C1	24.6	0.1061	3.0
C2	38.3	0.1533	3.3, 4.8
C3	54.3	0.2671	3.8, 7.6
C4	102.9	0.2715	3.9
C5	70.6	0.2407	3.4

[a] S_{BET} is the specific surface area calculated from the N_2 adsorption isotherm according to the BET method

[b] V_{total} is the single-point total pore volume

[c] D_{BJH} is the pore size determined from the N_2 desorption branch using the BJH model

in the interlayer region. The basicity of LDH required for reaction can then be achieved by intercalation of hydroxyl groups with controlled reconstruction process. Here, the reconstruction degree has pronounced effect on the basicity of LDH, which may be a key factor to affect the catalytic performance.

The basic properties of the series of Pd/LDH sample catalysts were investigated using the CO_2-TPD technique. Figure 4 shows that each profile includes three main overlapping peaks centred around 320, 420 and 480 °C, which can be assumed that at least three types of basic sites exist on the surface of the samples. According to Di Cosimo et al. [45], by deconvoluting the TPD profiles and integrating the three desorption peaks, which are referred to as α-(low temperature), β-(intermediate temperature) and γ-(high temperature), we could obtain the relative contributions from three types of adsorbed CO_2. The adsorbed

CO_2 quantity and the corresponding basic properties are listed in Table 2 for all catalyst samples. The total base amount (adsorbed CO_2 quantity) of the samples was significantly changed with the reconstruction condition. And the intermediate temperature peak is predominant on the Pd/LDH, representing most contribution of the total evolved CO_2. With increasing calcination temperature, the total percentage of the lower temperature peak and the intermediate temperature peak increased gradually, while that of the high temperature peak related to the strong base sites decreased (Table S1). This implies that not only the basic intensity but also the total basicity of the LDH support is affected by the regeneration degree of LDH structure. NH_3-TPD techniques were also carried out to measure the acidic properties of the series of Pd/LDH catalysts. From the contribution of the deconvoluting NH_3 desorption peaks (Fig. S2), we can see that the series of regenerated LDH supports possess different acidic sites; however, the catalysts exhibit similar contribution of the high temperature peak except the C5 sample (Table S2). Importantly, the total acidity amounts (adsorbed NH_3 quantity) of the samples have almost no difference with the controlled reconstruction condition (Table S2). The adsorbed NH_3 quantity and the corresponding acidic properties listed for all samples suggest that the catalysts possess relatively similar and fewer acidic sites number. It closely accords with the literatures [39, 46, 47] that the LDH was characterized to have a high Brønsted basicity associated with OH^- anions and a low Lewis acidity because of rehydration. Prinetto et al. [47] have reported that LDH could act as a solid base, which was as efficient as NaOH for the selective condensation reaction of acetone into diacetone-alcohol. Significant information was obtained from the ratios of the numbers of basic and acid sites, N_b/N_a (Table S2). It clearly evidenced the influence of the controlled reconstruction process on the basicity of samples: all the catalysts showed markedly high N_b/N_a ratios. In the present cases, the number of basic sites, N_b, showed a similar trend with respect to the N_b/N_a ratios. The results above indicate that different extent of reconstruction of LDH microcrystallites resulted in distinct difference in basicity, without apparent changes in acidity. Thus, the quantity of Brønsted (OH^-) basic sites required for reaction can be easily controlled by intercalation of hydroxyl groups with reconstruction and the regenerated LDH supports exhibit peculiar properties as Brønsted base.

3.3 The Effect of Calcination Temperature on Supported Pd Particles

The elemental analysis for Pd was performed by using ICP-ES measurement, revealing that the actual Pd weight percentage of the series of Pd/LDH catalysts was in good agreement with the nominal values of 1.06 wt%. The Pd particles distribution for the resulting Pd/LDH samples was determined by TEM observation by counting about 200

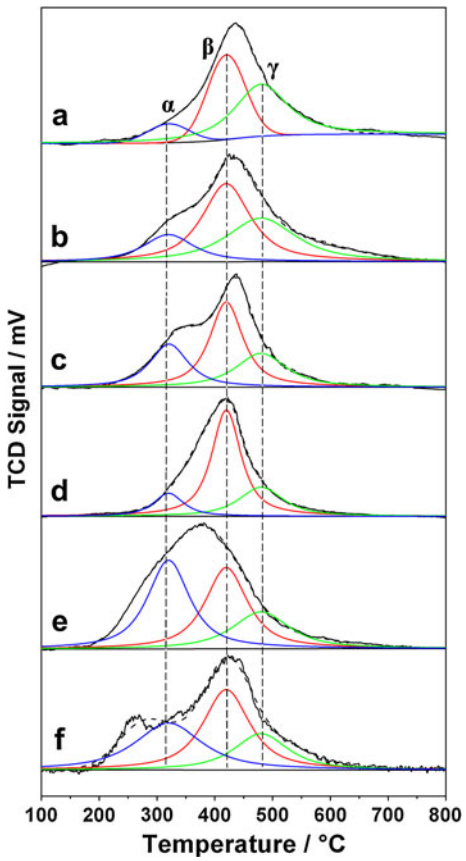

Fig. 4 CO_2-TPD curves of the LDH support (**a**) and the resulting Pd/LDH catalysts (**b**) C1, (**c**) C2, (**d**) C3, (**e**) C4, and (**f**) C5

Table 2 The initial conversion rate and the intrinsic TOF of the LDH support and the resulting Pd/LDH catalysts for the solvent-free aerobic oxidation of benzyl alcohol

Sample	Mean size of Pd (nm)	Basicity (mmol CO_2 g^{-1})	Initial conversion rate (mmol h^{-1})[a]	Intrinsic TOF (h^{-1})[b]
LDH	0	0.73	0	0
C1	6.4	0.81	4.1	412.9
C2	4.9	1.22	8.6	861.9
C3	4.2	1.60	9.6	964.1
C4	3.5	1.00	7.8	783.9
C5	2.6	0.66	6.0	603.8

Reaction conditions: catalyst 0.1 g; benzyl alcohol 48.5 mmol; O_2 atmosphere; temperature 100 °C

[a] Evaluated from the benzyl alcohol conversion at the initial reaction stage (conversion <20 %)

[b] Calculated from the initial conversion rate per Pd atom on the catalyst

particles in each case (Fig. 5). It is of interest that the centers of particle size distributions for the series of samples shift to the smaller values with increasing calcination temperature. For the C1 sample treated at a low temperature 100 °C, the size distribution was relatively broad. We could observe Pd particles with diameters from 2 to 12 nm, and the mean particle size of Pd was 6.4 nm. Relatively small particle size and narrow size distributions for the other samples calcinated at higher temperatures can be observed (Table 2). This may be caused by the stronger interaction between the ionic Pd species and the cationic LDH framework at higher calcination temperature. According to Zhang et al. [48], Pd^{II} species supported on NaY zeolite underwent gradual changes to $Pd^{2+}(OZ)_4$ (OZ = lattice oxygen of zeolite) with a rise in calcination temperature from 150 to 500 °C through UV–Vis and EXAFS investigations. We performed H_2-TPR studies for the Pd/LDH samples after calcination at different temperature in order to identify the changes of the ionic Pd species which might be reflected in the reduction behavior. The qualification of the reduction peaks in Fig. 6 for each sample revealed that these peaks corresponded to the reduction of Pd^{II} to Pd^0. When the calcination temperature increases from 100 to 500 °C, the main peaks for the reduction of PdO species shift to a higher temperature. This supports the idea that the interaction of the ionic Pd species and the LDH framework is closely related to the calcination temperature. The broader and asymmetric reduction peaks also indicate there may be different types of coordinations between the Pd species and the LDH framework. As the metal particles size is expected to be highly dependent on the relative nucleation rate and crystal growth during the reduction [49], the stronger interaction between the Pd species and LDH result in harder mobility and lower rate of nuclei growth, which would suppress the growth and cause the smaller size of Pd particles. Assuming that the present Pd particles are spherical shape in size range, the calculation model for the dispersion of Pd species in each sample is adopted with the following equation: Pd dispersion = 1.12/diameter (nm) [50]. The result shows that the Pd dispersion increases significantly with the calcination temperature, which is coincided with that the mean size of Pd particles decreases with increasing calcination temperature (Table S1). XPS study was also carried out to obtain the information of the state of Pd on catalyst samples (Fig. S3). Compared to the binding energy values of Pd 3d in pure palladium metal, the peaks with high intensity at around 335.3 and 340.3 eV, respectively, are assigned to the electron transitions of Pd $3d_{5/2}$ and Pd $3d_{3/2}$ of the Pd^0 particles dispersed on LDH. From the XPS result we can draw a conclusion that by this method we can obtain Pd^0 supported catalysts through one-step reaction with hydrazine hydrate reduction. The HRTEM experiments and the corresponding selected area electron diffraction (SAED) pattern were also performed to obtain more detailed information about the structure of Pd nanoparticles supported on the LDH. As can be seen from the HRTEM of C3 sample (Fig. 7a), the spacing of the crystallographic planes of 0.225 and 0.195 nm are in good agreement with the (111) and (200) lattice planes of the Pd particles, supporting the polycrystalline structure of those Pd particles. Such polycrystalline Pd particles are proved to be standard face-centred structure by the SAED pattern (Fig. 7b), in which the diffraction rings corresponding well to the (111) and (200) planes. Furthermore, the high-crystalline LDH support also exhibited (110) planes with hexagonal appearance in SAED pattern, which is consistent with the XRD results. In addition, it can be seen that the supported Pd particles tend to "sink" into the crystalline of LDH support, which could serve to improve the adhesion of metal particles and support and inhibit sintering at high temperatures.

3.4 Solvent-Free Oxidation of Benzyl Alcohol Over Pd/Ldh Samples

Catalytic performances of Pd/LDH samples for the solvent-free aerobic oxidation of benzyl alcohol are shown in Figs. 8 and 9. We confirmed that no conversion of benzyl alcohol occurred over the LDH support alone under the same reaction condition. For the series of Pd/LDH catalysts, the conversion increased with the reaction time and the selectivity to benzaldehyde decreased monotonically as the conversion was raised. We note that all the series of catalysts gave benzaldehyde in excellent selectivity (>97.6 %). It is interesting that the C3 sample with calcination temperature of 300 °C shows the highest catalytic activity among the series of Pd/LDH catalysts. Further, the comparison of the catalytic activity in Fig. 8 with the basicity and acidity (Table S2) of the Pd/LDH catalysts strongly suggests that both the mean diameter of Pd particles and the surface basicity of LDH support have remarkable influence on the catalytic activity.

To shed insight on the effect of Pd particle size and Brønsted basicity of LDH support on the intrinsic catalytic reactivity of Pd/LDH catalysts for the solvent-free aerobic oxidation of benzyl alcohol, great effort was taken to measure the initial conversion rate of benzyl alcohol at the beginning of the reaction (Table 2). For comparison of the different five Pd/LDH catalysts, we calculated the intrinsic TOF (moles of benzyl alcohol converted per mole of Pd per hour) based on the initial conversion rate and the Pd dispersion. It is clear that the intrinsic TOF depends significantly on the mean size of Pd particles and Brønsted basicity of LDH support. The catalysts with lower Brønsted basicity exhibit lower intrinsic TOF values in despite of

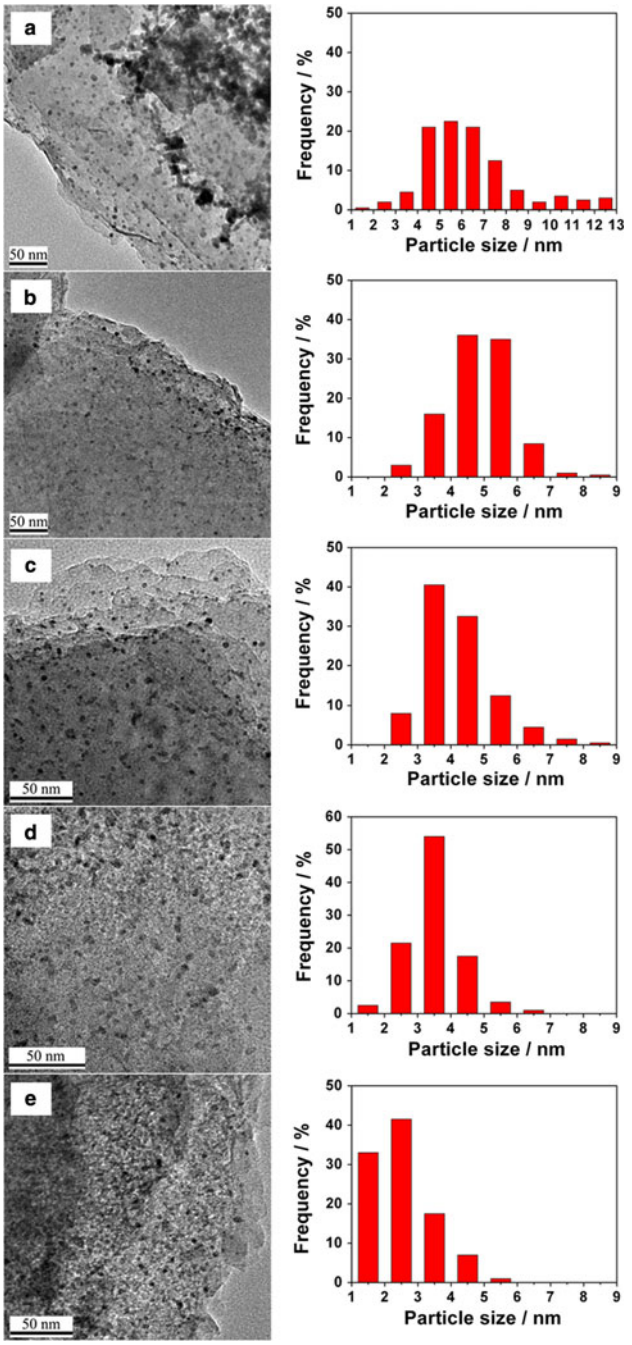

Fig. 5 TEM images and the corresponding Pd particles distribution of Pd/LDH catalysts (**a**) C1, (**b**) C2, (**c**) C3, (**d**) C4, and (**e**) C5

larger or smaller mean sizes of Pd particles. Many Pd-based catalysts have been reported to be very sensitive to the size of the Pd active phase for catalyzing organic reactions, such as hydrogenation of styrene [51], Suzuki coupling [52], and synthesis of vinyl acetate [53], are structure sensitive. Mori et al. [28] also compared the TOF of two representative supported catalysts with different size of Pd nanocluster for the aerobic oxidation, of which the smaller one exhibited much higher activity. Compared to the catalyst C1, we also obtained a smaller size of Pd particles sample (Fig. S4) with equal basicity, which was prepared similarly to the C1 catalyst except for changing the reducing agent to be KBH_4, and found that the smaller one behaved higher TOF (Table S3). Although smaller Pd particles with more coordinately unsaturated Pd sites are generally believed to be more active, our present observation indicates that the catalytic performance should be improved further with the cooperation of the support basicity. In comparison with catalyst C3, the catalyst C5 with smaller mean size of Pd particles shows obvious lower intrinsic TOF values. The catalyst C3 sample with more Brønsted basic sites of LDH support but medium Pd particle size shows the highest initial conversion rate and TOF values.

Much attention has been paid to the aerobic oxidation mechanism of alcohols catalyzed by heterogeneous Pd- or Ru-based catalysts [28, 54, 55]. In such heterogeneous catalytic systems, the formation of Pd- or Ru-alcoholate has been generally accepted for acting as the intermediate. Nevertheless, most reports of the alcohols oxidation with heterogeneous Pd catalysts proposed Pd^0 to be the active phase [28, 56]. According to Enache et al. [2] who investigated the supported Au–Pd catalysts for the oxidation of benzyl alcohol at 100 °C with O_2 as oxidant in the absence of solvent, the catalyst using Al_2O_3 support with basic property showed comparatively higher activity for the oxidation when compared with the SiO_2, carbon, and Fe_2O_3 supported samples. It was proposed that the oxidation may proceed through cooperation between the metal nanoparticles and basic sites on support. Very recently, Mitsudome et al. [57] proved the strongly positive effects of basic supports of LDH, Al_2O_3, and MgO on the deoxygenation over Au-based catalysts. Based on the above our experimental results and the previous findings of other groups, we propose a possible reaction pathway with Pd^0 nanoparticles as active sites (Scheme 1), which illustrating that the oxidation would proceed through cooperation between the Pd nanoparticles and Brønsted-base sites on LDH. Firstly, benzyl alcohol attacks a Brønsted-base site on the LDH, which passes through an abstraction of the proton by the hydroxyl group on the support, to form a water molecule and gives an alkoxide intermediate at the interface. Next, the intermediate undergoes co-ordination to form a Pd-H bond with the coordinately unsaturated Pd^0 active centre to afford unsteady Pd-alcoholate-LDH species, which undergoes a β-hydride elimination to give Pd-hydride species at the catalyst interface together with the corresponding carbonyl compound. Subsequent reaction of the hydride species with O_2 regenerate the Pd^0 specie, along with the formation of O_2 and H_2O, thereby completing the catalytic cycle.

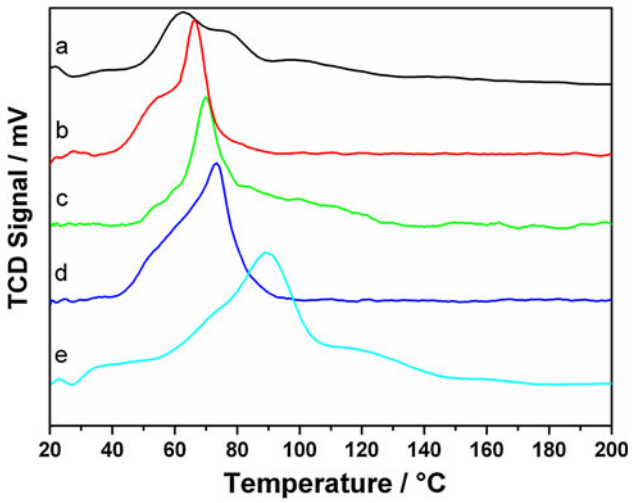

Fig. 6 H_2-TPR curves of the unreduced Pd^{II}/LDH catalysts with different calcination temperature (**a**) 100 °C, (**b**) 200 °C, (**c**) 300 °C, (**d**) 400 °C, and (**e**) 500 °C

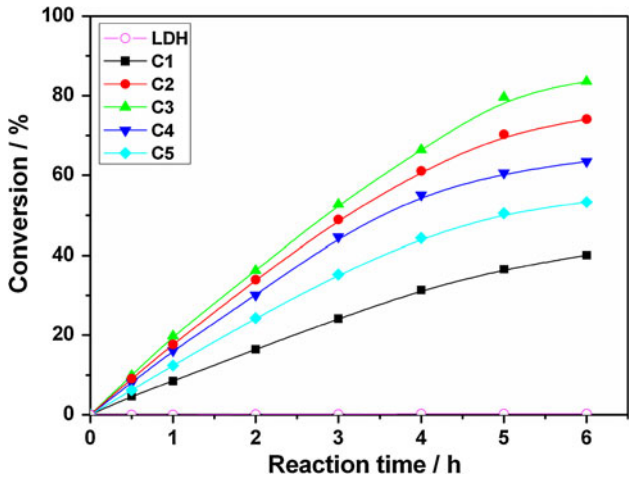

Fig. 8 The conversion of benzyl alcohol over the Pd/LDH catalysts (**a**) C1, (**b**) C2, (**c**) C3, (**d**) C4, and (**e**) C5

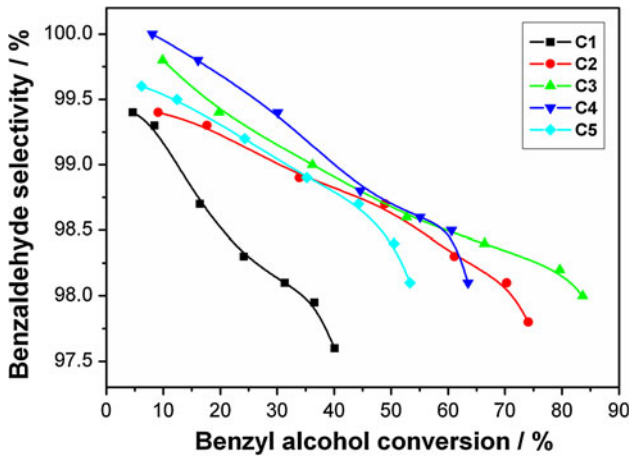

Fig. 9 The selectivity to benzaldehyde during the oxidation of benzyl alcohol over the Pd/LDH catalysts (**a**) C1, (**b**) C2, (**c**) C3, (**d**) C4, and (**e**) C5

Further, the following experiments of benzyl alcohol described below also provided some insights to support the above reaction pathway. Firstly, our present catalytic system was determined not to contain any free radical intermediates. Both the conversion and selectivity in the oxidation of benzyl alcohol was hardly influenced when the reaction medium involved a radical trap (2,6-di-tert-butyl-*p*-cresol). Secondly, the molecular oxygen was quantitatively used as the oxidant for the oxidative dehydrogenation. The consumption of O_2 gas was measured, and a ca. 1:2 ratio of the O_2 uptake to benzaldehyde yield was observed. When KI-containing starch was used to detect the formation of H_2O_2 qualitatively for the present system at ca. 50 % conversion, it was interesting to find the color changed slightly from light yellow to blue. In consequence the formed O_2 and H_2O may originate from the likely intermediate of H_2O_2, which was similar to the literatures [28, 58]. Thirdly, the initial oxidation rates of benzyl alcohol exhibited no difference with the change of oxygen partial pressure at 0.2 (air), 1.0, and 3.0 atm, which were independent of the O_2 pressure. When the catalyst was removed after reaction of 2 h (about 40 % conversion of

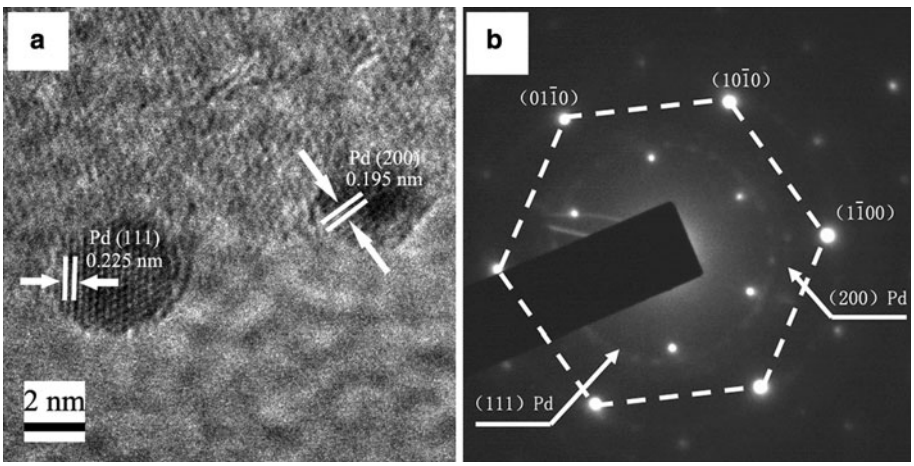

Fig. 7 HRTEM image (**a**) and the corresponding selected area electron diffraction pattern (**b**) of the Pd/LDH catalyst with calcination temperature 300 °C (C3)

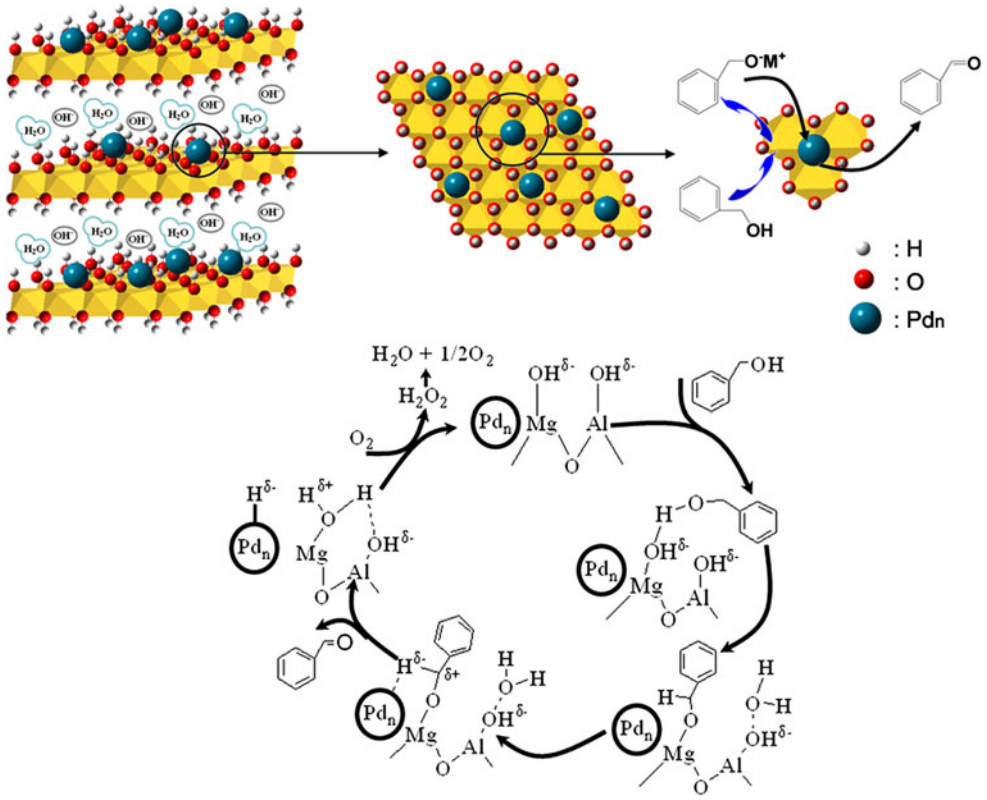

Scheme 1 The possible reaction pathway of the oxidation for benzyl alcohol over Pd/LDH sample

the alcohol for C3 catalyst), the filtered solution was allowed to react for 3 h under 1 atm O_2, but no further oxidation was observed, which indicated the present alcohol oxidation was indeed proceeding at the interface between the solid catalyst and the liquid phase. Furthermore, benzaldehyde was obtained only in a small amount over the Pd/LDH catalyst under N_2 atmosphere, presumably due to the presence of residual O_2. Finally, the kinetic data ($K_M = 11.69$ M, $k_2 = 4.73$ h^{-1}) of oxidation could be well accommodated with a rate equation based on the Michaelis–Menten type model for the proposed mechanism (Eq. 1) and the kinetic isotope effect for intramolecular competitive oxidation (2.8) is also consistent with those obtained for other systems [59, 60], which strongly implies the abstraction of β-hydride from the Pd-alcoholate-LDH species is a rate-determining step of the catalytic oxidation cycle and the H-atom elimination mechanism is reasonable.

$$\text{LDH-Pd} + \text{PhCH}_2\text{OH} \underset{k_{-1}}{\overset{k_1}{\rightleftharpoons}} \text{LDH----Pd}(\text{OCH}_2\text{Ph}) \xrightarrow{k_2} \text{LDH-Pd-H} + \text{PhCHO} \quad (1)$$

Our observation that the benzyl alcohol oxidation was determined by the mean size of Pd nanoparticles and the Brønsted-base sites on the LDH implied that their existing a cooperation of them for the catalytic aerobic oxidation of benzyl alcohol. This allows us to further consider that the Brønsted-base site on the LDH facilitates β-hydrogen elimination from the metal–alkoxide intermediate, thus leading to strong enhancement of activity for supported Pd particles in benzyl alcohol oxidation. Removing the water molecule that binds the Pd active centre and Brønsted-base site improves the situation of the Pd species during β-hydrogen elimination by, for example, producing a coordinately unsaturated Pd site. As a consequence of the well known formation of metal-hydride species in the alcohol oxidation [59], the distinguished oxidation activities of Pd particles should be attributed to their unique reactivity towards a metal–alkoxide intermediate. Also, the solid LDH support can promote the oxidation as a Brønsted base as well as stabilize these Pd particles.

Furthermore, Table 3 compares the catalytic performance of the active Pd/LDH catalyst (sample C3) with the non-basic Pd/SiO_2 and Pd/Al_2O_3 catalyst as well as other reported catalysts for the aerobic oxidation of benzyl alcohol. Although the experimental conditions used in various studies deviate somehow, a rough comparison is still feasible. The C3 catalyst, exhibiting a specific rate of

Table 3 Comparison of the catalytic performance of the resulting Pd/LDH catalyst sample (C3) with those of the reported catalyst samples employed in the aerobic oxidation of benzyl alcohol

Catalyst	TOF (h^{-1})	Temperature (°C)	Pressure (10^5 Pa)	Solvent	Reference
Pd/LDH (C3)[a]	964	100	1	None	This work
Pd/SiO_2[a]	39	100	1	None	This work
Pd/Al_2O_3[a]	165	100	1	None	This work
$Pd(OAc)_2(py)_2$/LDH	10	80	1	$PhCH_3$	[30]
$[Pd(OH)_4]^{2-}$/LDH	50	80	1	$PhCF_3$	[31]
Pd/SiO_2[b]	26	70	1	None	[61]
Pd/hydroxyapatite	495	90	1	$PhCF_3$	[62]
Pd/bathophenanthroline	35	100	30	Water	[63]
Pd/carbon	5	60	1.5	$PhCH_3$	[64]
Pd/NaX	626	100	1	None	[56]
$AuPd/TiO_2$	6190	100	1	None	[2]
Au/TiO_2	213	100	2	None	[2]
$Au/\alpha\text{-}Ga_2O_3$	125	130	5	None	[65]
Au/Fe_2O_3	18	130	5	None	[65]
Au/MnO_2	320	120	3	None	[66]
Ru/Al_2O_3	97	90	25	$PhCH_3$	[67]
RuCo/HAP	78	90	1	$PhCH_3$	[68]
Ru/HAP-Cl[c]	233	80	1	$PhCH_3$	[69]

[a] Reaction conditions: catalyst C3 0.1 g; benzyl alcohol 48.5 mmol; O_2 atmosphere; temperature 100 °C; time 6 h. TOF was measured after reaction time of first 1 h

[b] H_2 reduction

[c] Halogenous hydroxyapatite

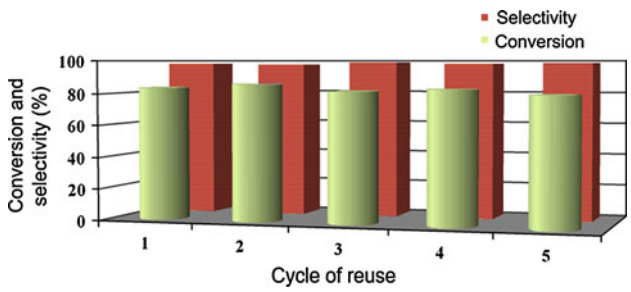

Fig. 10 Reuse of the Pd/LDH catalyst with calcination temperature 300 °C (C3): the conversion of benzyl alcohol and the selectivity to benzaldehyde

964 h^{-1} compares favorably with Pd/SiO_2 and Pd/Al_2O_3 catalyst as well as the results reported on the other Au-, Ru- and Pd-based catalysts, demonstrating a significant potential of present catalytic system. Moreover, we mention that most reported catalyst systems require additional bases, electron/proton transfer mediators, and high O_2 pressure. Our Pd/LDH catalyst, however, does not need any additives or co-catalysts to facilitate its efficient catalytic cycle under an atmospheric O_2 pressure.

Subsequently, we explored the C3 catalyst from the issues of deactivation and reusability, which are highly desirable for industrial application. To test this, a series of five consecutive reactions were carried out with the same C3 catalyst sample, which still gave excellent yields of benzaldehyde in the last run (Fig. 10). After the reaction, the catalyst of the reaction mixture was filtered, collected and analyzed by ICP-ES. A very low amount of palladium was leached from the reaction, and there was only a little change from 1.06 to 0.99 % of Pd loading after 5 cycles of reaction. The preservation of catalytic activity and the facile recycling of C3 sample in the oxidation reaction were probably due to the very low loss of Pd active sites. Clearly, the morphology and crystalline structure of the LDH support was mostly retained, and no obvious agglomeration of palladium was observed on the support surface after the fifth reaction (Fig. S5a). The TEM image (Fig. S5b, c) shows that the size of Pd particles and the corresponding particle size distribution of the recovered C3 catalyst have been well preserved during/after the course of oxidation reaction, with the mean particle size about 4.3 nm. Hence, the results presented above show that the C3 catalyst is an active and stable heterogeneous catalyst for the oxidation of benzyl alcohol, with the whole process efficient and environmentally friendly.

4 Conclusions

In conclusion, we have demonstrated a new and green catalytic methodology for the oxidation of benzyl alcohol

over Pd particles supported on MgAl–OH^-–LDH support in the solvent-free liquid phase using molecular oxygen as oxidizing reagents. On the basis of characterization by physicochemical methods, it was found that the layered structure of LDH could be reconstructed to different extent under control by calcination and rehydration in ethanol aqueous solution, which presented changing numbers of Brønsted-base sites. The calcination temperature imposed a restricted nano-size on the supported Pd particles under identical reduction of hydrazine hydrate, which demonstrated a convenient approach to control the size of Pd nanoparticles on LDH surface. The sample with a larger amount of Brønsted-base sites of LDH support is more active for the oxidation of benzyl alcohol, and after five catalytic runs it still gives benzaldehyde in excellent yields. The promotional effect of the Brønsted-base sites of the LDH support on the catalytic activity for benzyl alcohol oxidation over Pd/LDH is discussed. It is reasonable to consider that the mean size of Pd particles and the Brønsted basicity of supports are the essential factors to determine the intrinsic TOF for the Pd/LDH samples.

Acknowledgments We acknowledge generous financial support from the National Natural Science Foundation of China and the 973 Program (No. 2011CBA00506).

References

1. Mallat T, Baiker A (2004) Chem Rev 104:3037
2. Enache DI, Edwards JK, Landon P, Solsona-Espriu B, Carley AF, Herzing AA, Watanabe M, Kiely CJ, Knight DW, Hutchings GJ (2006) Science 311:362
3. Serra M, Salagre P, Cesteros Y, Medina F, Sueiras JE (2002) J Catal 209:202
4. Cabello FM, Tichit D, Coq B, Vaccari A, Dung NT (1997) J Catal 167:142
5. Gluhoi AC, Marginean P, Stanescu U (2005) Appl Catal A 294:208
6. Grzechowiak JR, Szyszka I, Rynkowski J, Rajski D (2003) Appl Catal A 247:193
7. Chupin J, Gnep NS, Lacombe S, Guisnet M (2001) Appl Catal A 206:43
8. Scire S, Minico S, Crisafulli C (2002) Appl Catal A 235:21
9. Homeyer ST, Karpinski Z, Sachtler WMH (1990) J Catal 123:60
10. Besoukhanova C, Guidot J, Barthomeuf D, Breysse M, Bernard JR (1981) J Chem Soc Faraday Trans 77:1595
11. Lashdaf M, Nieminen VV, Tiitta M, Venalainen T, Osterholm H, Krause O (2004) Microporous Mesoporous Mater 75:149
12. Hu S, Xue M, Chen H, Shen J (2010) Chem Eng J 162:371
13. Liu HZ, Jiang T, Han BX, Liang SG, Zhou YX (2009) Science 326:1250
14. Zhu JJ, Figueiredo JL, Faria JL (2008) Catal Commun 9:2395
15. Basile F, Vaccari A, Rives V (2001) Layered double hydroxides: present and future. Nova Science Publishers, New York
16. Williams GR, O'Hare D (2006) J Mater Chem 16:3065
17. Evans DG, Duan X (2006) Chem Commun 2006:485
18. Manzi-Nshuti C, Wang D, Hossenlopp JM, Wilkie CA (2008) J Mater Chem 18:3091
19. Woo MA, Song MS, Kim TW, Kim IY, Ju JY, Lee YS, Kim SJ, Choy JH, Hwang SJ (2011) J Mater Chem 21:4286
20. Oh JM, Choi SJ, Lee GE, Han SH, Choy JH (2009) Adv Funct Mater 19:1617
21. Khan SB, Liu C, Jang ES, Akhtar K, Han H (2011) Mater Lett 65:2923
22. Combourieu B, Inacio J, Delort AM, Forano C (2001) Chem Commun 2001:2214
23. Williams GR, O'Hare D (2005) Chem Mater 17:2632
24. Sels BF, De Vos DE, Jacobs PA (2001) Catal Rev Sci Eng 43:443
25. Tichit D, Coq B (2003) Cattech 7:206
26. Roeffaers MBJ, Sels BF, Uji-i H, De Schryver FC, Jacobs PA, De Vos DE, Hofkens J (2006) Nature 439:572
27. Climent MJ, Corma A, Iborra S, Velty A (2004) J Catal 221:474
28. Mori K, Hara T, Mizugaki T, Ebitani K, Kaneda K (2004) J Am Chem Soc 126:10657
29. Nishimura T, Kakiuchi N, Inoue M, Uemura S (2000) Chem Commun 2000:1245
30. Kakiuchi N, Maeda Y, Nishimura T, Uemura S (2001) J Org Chem 66:6620
31. Hara T, Ishikawa M, Sawada J, Ichikuni N, Shimazu S (2009) Green Chem 11:2034
32. Tsunoyama H, Sakurai H, Negishi Y, Tsukuda T (2005) J Am Chem Soc 127:9374
33. Karimi B, Zamani A, Clark JH (2005) Organometallics 24:4695
34. Choudhary D, Paul S, Rajive GA, Clark JH (2006) Green Chem 8:479
35. ten Brink GJ, Arends IWCE, Sheldon RA (2000) Science 287:1636
36. Urgoitia G, SanMartin R, Herrero MT, Dominguez E (2011) Green Chem 13:2161
37. Ishida T, Nagaoka M, Akita T, Haruta M (2008) Chem Eur J 14:8456
38. Fang W, Chen J, Zhang Q, Deng W, Wang Y (2011) Chem Eur J 17:1247
39. Lei X, Zhang F, Yang L, Guo X, Tian Y, Fu S, Li F, Evans DG, Duan X (2007) AIChE J 53:932
40. Adachi-Pagano M, Forano C, Besse JP (2003) J Mater Chem 13:1988
41. Ogawa M, Kaiho H (2002) Langmuir 18:4240
42. Bakala PC, Briot E, Millot Y, Piquemal JY, Brégeault JM (2008) J Catal 258:61
43. Tichit D, Lutic D, Coq B, Durand R, Teissier R (2003) J Catal 219:167
44. Roelofs JCAA, van Dillen AJ, de Jong KP (2000) Catal Today 60:297
45. Di Cosimo JI, Apesteguía CR, Ginés MJL, Iglesia E (2000) J Catal 190:261
46. Prinetto F, Ghiotti G, Durand R, Tichit D (2000) J Phys Chem B 104:11117
47. Prinetto F, Tichit D, Teissier R, Coq B (2000) Catal Today 55:103
48. Zhang Z, Sachtler WMH, Chen H (1990) Zeolites 10:784
49. Homeyer ST, Sachtler WMH (1989) J Catal 117:91
50. Mahata N, Vishwanathan V (2000) J Catal 196:262
51. Veisz B, Kiraly Z, Toth L, Pecz B (2002) Chem Mater 14:2882
52. Li Y, Boone E, El-Sayed MA (2002) Langmuir 18:4921
53. Han YF, Kumar D, Goodman DW (2005) J Catal 230:353
54. Yamaguchi K, Mizuno N (2002) Angew Chem Int Ed 41:4538
55. Pillai UR, Sahle-Demessie E (2004) Green Chem 6:161
56. Li F, Zhang QH, Wang Y (2008) Appl Catal A 334:217
57. Mitsudome T, Noujima A, Mikami Y, Mizugaki T, Jitsukawa K, Kaneda K (2010) Angew Chem Int Ed 49:5545
58. Steinhoff BA, Fix SR, Stahl SS (2002) J Am Chem Soc 124:766
59. Yamaguchi K, Mizuno N (2003) Chem Eur J 9:4353
60. Missen RW, Mims CA, Saville BA (1999) Introduction to chemical reaction engineering and kinetics. Wiley, New York

61. Chen J, Zhang QH, Wang Y, Wan HL (2008) Adv Synth Catal 350:453
62. Mori K, Yamaguchi K, Hara T, Mizugaki T, Ebitani K, Kaneda K (2002) J Am Chem Soc 124:11572
63. Arends I, ten Brink GJ, Sheldon RA (2006) J Mol Catal A 251:246
64. Dimitratos N, Villa A, Wang D, Porta F, Su DS, Prati L (2006) J Catal 244:113
65. Su FZ, Chen M, Wang LC, Huang XS, Liu YM, Cao Y, He HY, Fan KN (2008) Catal Commun 9:1027
66. Wang LC, He L, Liu Q, Liu YM, Chen M, Cao Y, He HY, Fan KN (2008) Appl Catal A 344:150
67. Zotova N, Hellgardt K, Kelsall GH, Jessiman AS, Hii KK (2010) Green Chem 12:2157
68. Opre Z, Grunwaldt JD, Maciejewski M, Ferri D, Mallat T, Baiker A (2005) J Catal 230:406
69. Zhang YJ, Wang JH, Yin J, Zhao KF, Jin CZ, Huang YY, Jiang Z, Zhang T (2010) J Phys Chem C 114:16443